JOURNAL OF
Applied Polymer
SCIENCE

Special Issue: Polymers for Microelectronics

Guest Editors: Dr Brian Knapp (Promerus LLC) and
Prof. Paul A. Kohl (Georgia Institute of Technology)

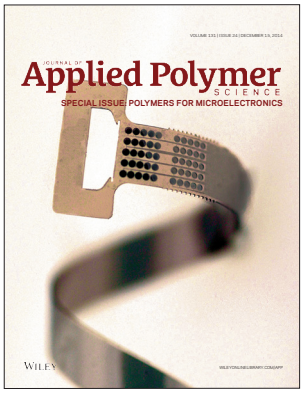

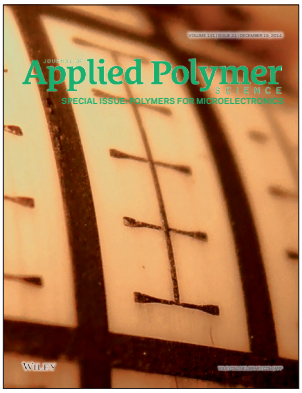

EDITORIAL

Polymers for Microelectronics
B. Knapp and P. A. Kohl, *J. Appl. Polym. Sci.* 2014, **DOI: 10.1002/app.41233**

REVIEW

Negative differential conductance materials for flexible electronics
A. Nogaret, *J. Appl. Polym. Sci.* 2014, **DOI: 10.1002/app.40169**

RESEARCH ARTICLES

Generic roll-to-roll compatible method for insolubilizing and stabilizing conjugated active layers based on low energy electron irradiation
M. Helgesen, J. E. Carlé, J. Helt-Hansen, A. Miller, and F. C. Krebs, *J. Appl. Polym. Sci.* 2014, **DOI: 10.1002/app.40795**

Selective etching of polylactic acid in poly(styrene)-block-poly(D,L)lactide diblock copolymer for nanoscale patterning
C. Cummins, P. Mokarian-Tabari, J. D. Holmes, and M. A. Morris, *J. Appl. Polym. Sci.* 2014, **DOI: 10.1002/app.40798**

Preparation and dielectric behavior of polyvinylidene fluoride composite filled with modified graphite nanoplatelet
P. Xie, Y. Li, and J. Qiu, *J. Appl. Polym. Sci.* 2014, **DOI: 10.1002/app.40229**

Design of a nanostructured electromagnetic polyaniline–Keggin iron–clay composite modified electrochemical sensor for the nanomolar detection of ascorbic acid
R. V. Lilly, S. J. Devaki, R. K. Narayanan, and N. K. Sadanandhan, *J. Appl. Polym. Sci.* 2014, **DOI: 10.1002/app.40936**

Synthesis and characterization of novel phosphorous-silicone-nitrogen flame retardant and evaluation of its flame retardancy for epoxy thermosets
Z.-S. Li, J.-G. Liu, T. Song, D.-X. Shen, and S.-Y. Yang, *J. Appl. Polym. Sci.* 2014, **DOI: 10.1002/app.40412**

Electrical percolation behavior and electromagnetic shielding effectiveness of polyimide nanocomposites filled with carbon nanofibers
L. Nayak, T. K. Chaki, and D. Khastgir, *J. Appl. Polym. Sci.* 2014, **DOI: 10.1002/app.40914**

Morphological influence of carbon modifiers on the electromagnetic shielding of their linear low density polyethylene composites
B. S. Villacorta and A. A. Ogale, *J. Appl. Polym. Sci.* 2014, **DOI: 10.1002/app.41055**

Electrical and EMI shielding characterization of multiwalled carbon nanotube/polystyrene composites
V. K. Sachdev, S. Bhattacharya, K. Patel, S. K. Sharma, N. C. Mehra, and R. P. Tandon, *J. Appl. Polym. Sci.* 2014, **DOI: 10.1002/app.40201**

Anomalous water absorption by microelectronic encapsulants due to hygrothermal-induced degradation
M. van Soestbergen and A. Mavinkurve, *J. Appl. Polym. Sci.* 2014, **DOI: 10.1002/app.41192**

Design of cyanate ester/azomethine/ZrO_2 nanocomposites high-k dielectric materials by single step sol-gel approach
M. Ariraman, R. Sasi Kumar and M. Alagar, *J. Appl. Polym. Sci.* 2014, **DOI: 10.1002/app.41097**

Furan/imide Diels–Alder polymers as dielectric materials
R. G. Lorenzini and G. A. Sotzing, *J. Appl. Polym. Sci.* 2014, **DOI: 10.1002/app.40179**

High dielectric constant polyimide derived from 5,5'-bis[(4-amino) phenoxy]-2,2'-bipyrimidine
X. Peng, Q. Wu, S. Jiang, M. Hanif, S. Chen, and H. Hou, *J. Appl. Polym. Sci.* 2014, **DOI: 10.1002/app.40828**

The influence of rigid and flexible monomers on the physical-chemical properties of polyimides
T. F. da Conceição and M. I. Felisberti, *J. Appl. Polym. Sci.* 2014, **DOI: 10.1002/app.40351**

JOURNAL OF Applied Polymer SCIENCE

Special Issue: Polymers for Microelectronics

Guest Editors: Dr Brian Knapp (Promerus LLC) and
Prof. Paul A. Kohl (Georgia Institute of Technology)

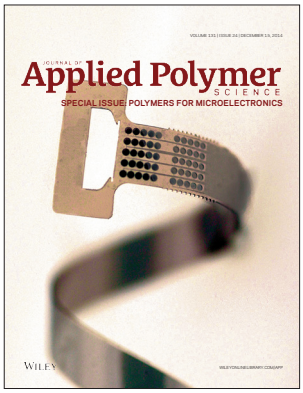

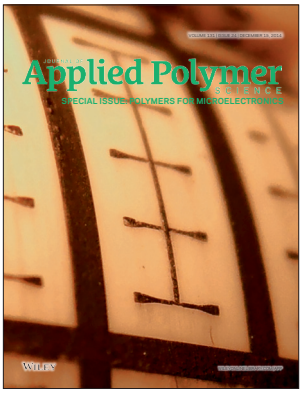

Journal of Applied Polymer Science

Morphological Influence of Carbon Modifiers on the Electromagnetic Shielding of Their Linear Low Density Polyethylene Composites

Byron S. Villacorta, Amod A. Ogale
Department of Chemical Engineering and Center for Advanced Engineering Fibers and Films, Clemson University, South Carolina 29634-0909
Correspondence to: A. A. Ogale (E-mail: ogale@clemson.edu)

ABSTRACT: The influence of morphology of carbon modifiers on the electrical, thermal, and mechanical properties of their polyethylene-matrix composites is reported. Four heat-treated (HT) carbon modifiers were investigated: PR-19-HT carbon nanofibers, multiwalled carbon nanotubes (MWNT-HT), helical multiwalled carbon nanotubes (HCNT-HT), and mesophase pitch-based P-55 carbon fibers as a control. These were melt-mixed with linear low density polyethylene at 10 vol %, which was above the percolation threshold. The electromagnetic shielding effectiveness (EM SE) of the composites exhibits significant dependence on the modifier morphology. Thus, MWHTs, with the highest aspect ratio, lead to the highest composite electrical and thermal conductivities (34 Sm^{-1} and 1 Wm^{-1} K^{-1}) and EM SE (~24 dB). In contrast, HCNT, due to their coiled shape and low aspect ratio, lead to segregated microstructure and low EM SE (<1 dB). However, these composites display the highest ductility (~250%) and flexibility, probably due to matrix-modifier mechanical bonding provided by the helical morphology. © 2014 Wiley Periodicals, Inc. J. Appl. Polym. Sci. **2014**, *131*, 41055.

KEYWORDS: composites; graphene and fullerenes; microscopy; morphology; nanotubes; X-ray

Received 15 April 2014; accepted 27 May 2014
DOI: 10.1002/app.41055

INTRODUCTION

For proper functioning of electronic devices, electromagnetic shielding effectiveness (EM SE) and electrostatic discharge (ESD) protection must be provided for attaining electromagnetic compatibility.[1,2] EM SE is typically provided by conductive materials that reflect and/or absorb the interfering electromagnetic signals. Thus, by means of such barriers, susceptible circuitry components are protected or electromagnetic emissions from radiating components can be contained.[2–4] Conductive materials are also used to provide ESD protection, avoiding the accumulation of charge by supplying a safe path for charge dissipation.[5]

Conductive composites and hybrid materials have been demonstrated as suitable substitutes of metallic materials due to their versatile properties.[1,6] In fact, it is widely known that different electrically conductive modifiers can be added to polymers to form electrical networks within the polymeric matrix.[7–12] Such network formation improves the lossy transport properties of the material (i.e., electrical conductivity and imaginary permittivity), which directly influence electromagnetic shielding.[4,13] Conductive carbon nanomodifiers, such as carbon nanofibers and nanotubes, are particularly attractive due to their nanosize, excellent conductivity, low density and corrosion resistance, which enables the manufacturing of conductive thin-wall structures such as films, fibers and microinjection molded parts.[13–15]

Literature studies indicate that, for a given graphitic crystallinity of the carbon modifiers and fixed melt-mixing conditions, the attained level of modifier-modifier interconnection will generally depend on the following morphological features of the modifiers: aspect ratio, shape, and diameter.[15–19] The modifier diameter influences the level of intermolecular interactions (van der Waals and London dispersion forces) among the modifiers, whereas the other two are primarily geometrical factors that directly lead to the formation of entanglements.[20,21] Thus, because the intermodifier connection level will determine the cluster size distribution, and as a result, the level of electrical percolation (i.e., macroconduction mechanism), these morphological factors will define the type of electrical network formed in the composite.[22] Also, we have reported the influence of the morphological features (shape and surface) of carbon nanofibers on the electrical conductivity and tensile properties of their polyethylene composites.[23] However, the effect of different carbon-based nanomorphologies on the electromagnetic shielding of their polyethylene nanocomposites has not been fully

investigated. Therefore, this study reports on the effect of three heat-treated (HT) carbon nanomodifiers on the EM SE of their composites prepared by melt-mixing with a flexible linear low-density polyethylene matrix. Mesophase pitch-based carbon fibers (CF, P-55), which possess a reasonable graphitic content (as opposed to PAN-based CF) were also included in this study as a control sample, that is, with the purpose of comparing micromorphologies vs. nanomorphologies. The microstructural, electrical, thermal, and mechanical properties of these composites are reported in relation to their electromagnetic shielding performance.

EXPERIMENTAL

Materials

The matrix polymer used throughout this study was poly(ethylene-*co*-1-octene, Dowlex™ 2045), a film grade flexible linear low density polyethylene (LLDPE). It has a DSC melting point of 122°C and melt flow index of 1 g/10 min (190°C/2.16 kg, ASTM D1238). Carbon nanofibers, Pyrograf® III PR-19 (Applied Science), straight (MWNT), and helical multiwalled carbon nanotubes (HCNT) from CheapTubes, were used as nanomodifiers. PR-19 CNFs were produced by chemical vapor deposition (CVD) from natural gas precursor by using a Fe-sulfide catalyst at about 900°C.[24,25] MWNT were also produced by CVD from methane with a Ni-Fe catalyst, whereas HCNT were produced from C_2H_2 precursor by CVD at 500°C with a Fe_2O_3 catalyst.[26] Mesophase pitch-based Cytec Thornel® P-55 short CF were included as "micro" modifiers (diameter ~10 μm, length: 100–500 μm).

The intrinsic electrical conductivity of the modifier phase is an important factor in determining the electrical properties of the resulting composites.[27,28] This conductivity, in turn, is a strong function of its graphitic crystallinity, which can be increased by heat-treating the nanomodifiers to temperatures exceeding 2000°C as demonstrated in previous studies.[24,25,27] Therefore, ultra-high temperature heat treatment (HT) at 2500°C was carried out for all of the as-received nanomodifiers in a Thermal Technology HP50-7010 furnace in helium atmosphere prior to compounding.[28]

Processing

The nanocomposites were prepared by an optimized soft melt-mixing of LLDPE with 10 vol % of each of the four types of modifiers using a Haake Rheomix 600 batch mixer (BM) at 190°C and 20 rpm for 2 min.[26,29] The composites were processed by thermal compaction at 190°C into circular sheets about 2.5 mm thick and 133 mm diameter using a Carver laboratory press. Two specimens were independently mixed and compacted per concentration (replicates, $n = 2$).

Carbon Modifier Characterization

Scanning electron microscopy (SEM Hitachi S-4800) was conducted on the heat-treated (HT) modifiers. At least 10 different micrographs at different levels of magnification were captured per modifier type. From the high-magnification SEM micrographs, the length and diameter measurements of the modifiers were carried out using image analysis (ImagePro®). For each modifier type, a set of at least 150 representative imaged modifiers were measured to obtain statistical significance. From the low-magnification SEM micrographs, the level of initial clustering of the nanomodifiers was also obtained by image analysis.

Raman spectroscopy was conducted on the modifiers to analyze the disordered (D) and graphitic (G) bands observed in carbon materials at about 1300 and 1600 cm^{-1}, respectively. A Renishaw micro-Raman spectroscope equipped with a 785 nm wavelength diode laser was used. The WiRE software (version 3.2) was used to analyze the peaks to determine the I_D/I_G Raman area ratio.[24] A replication of eight was used ($n = 8$). X-ray diffraction (XRD, Rigaku Ultima IV X-ray diffractometer) was also conducted on the HT carbon modifiers using Cu target Kα radiation with a wavelength of 1.5406 Å.[24] A Bragg's angle sweep from 20° to 30° at a rate of 0.75° min^{-1} was used for all measurements. The Ultima IV X-ray source was operated at 40 kV and 44 mA. A replication of 3 was used for all XRD experiments ($n = 3$).

The bulk electrical conductivity (BEC) of the modifiers was measured using a Keithley 196 System while compressing the modifiers in an insulating fixture at a compaction stress of 50 MPa.[30] The bulk thermal diffusivity of the nanomodifiers was measured using a NETZSCH Laser Flash Analyzer LFA 447 (ASTM E1461). Compacted pellets of 2 mm thickness and 12.7 mm diameter made out of the nanomodifiers were analyzed. The bulk thermal conductivity was calculated from the bulk thermal diffusivity, bulk density measurements, and the heat capacity obtained from a simple rule of mixture for the modifiers and air (pellet replicates, $n = 2$).

Composites Characterization

The morphology of the composites was assessed by inspection of the cross-section of the cryo-fracturated composites using scanning electron microscopy (Hitachi S-4800, Hitachi SU-6600). For each type of composite, five different macroscopic locations were investigated. For each location, five different spots were imaged. After a soft dilution of the 10 vol % composites with LLDPE to 1 vol %, carried out in the BM at 20 rpm, 190°C for 2 min, the composites became transparent enough to conduct transmission light microscopy (LM, BX60 Olympus Optical Microscope). Seven different locations on the surface of about 100 μm thick composite films were inspected for each composite type (nominally 4 mm^2 of inspected area) to measure the average diameter and area of the clusters.

The DC in-plane volume electrical conductivity of the nanocomposites was measured using a Keithley 6517B High Resistance Meter (1 pA−20 mA) connected to a Keithley 8002A Resistivity Test Fixture modified with external electrodes (ASTM D257). The measurements were performed with help of the Keithley 6524 software by which a DC voltage of ± 5 V was applied across the highly conductive composite samples and ± 50 V across the less conductive samples. The conductivity was obtained from resistance measurements of specimens that were 12.5 mm wide, 2.5 mm thick, and about 20 mm long. Silver paint was applied on the surfaces at each end of the samples and their in-plane resistance was measured (replicates $n = 4$).

The NETZSCH LFA 447 was used to measure the through-plane thermal diffusivity of the composites. Four square

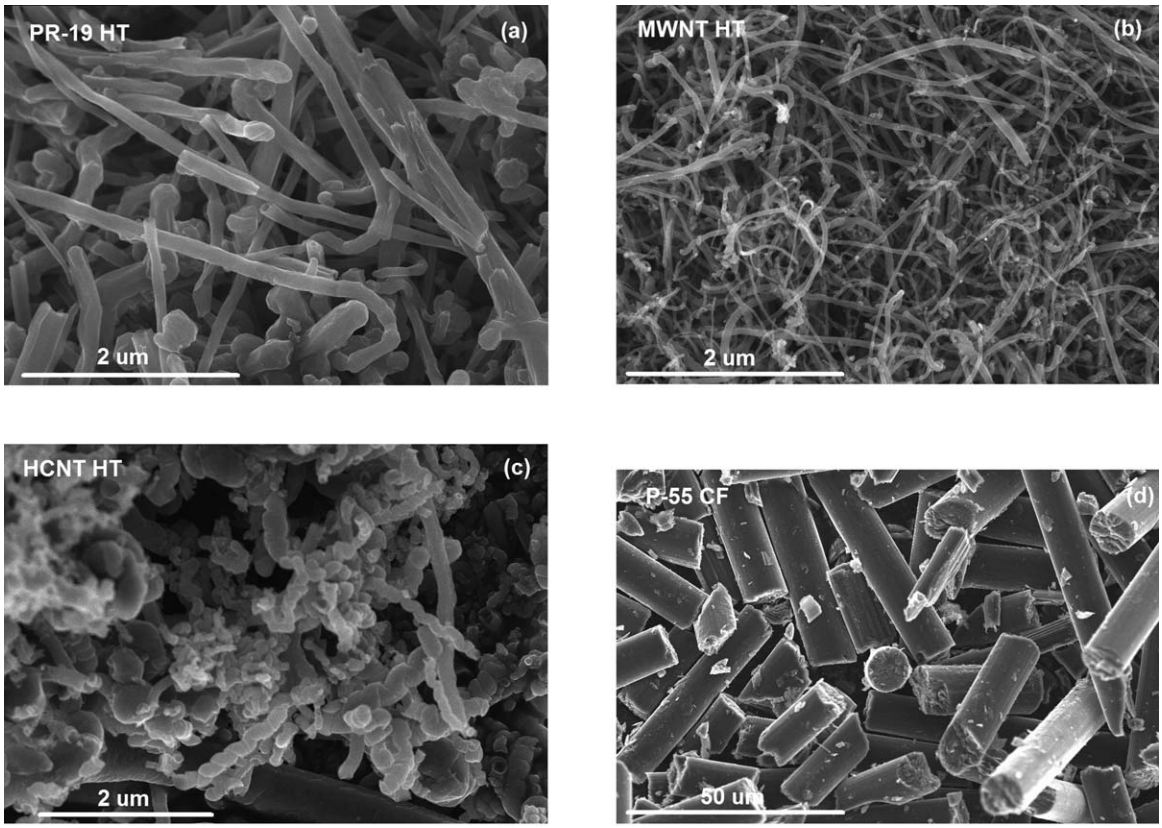

Figure 1. Representative scanning electron micrographs (SEM) of the HT carbon modifiers used to prepare the composites.

specimens of 10 × 10 mm^2 and about 0.5 mm thick were cut per composite type ($n = 4$). From mixing rules, the heat capacity and density of the composites were calculated, enabling the estimation of their composite thermal conductivity.

The complex electrical permittivity (real ε' and imaginary ε'') of the nanocomposites, in their sheet form (2.5 mm thick), was measured utilizing an Agilent 4291B RF Impedance/Material Analyzer and an Agilent 16453A Dielectric Material Test Fixture. Prior to the measurements the analyzer was calibrated using an Agilent calibration kit [short (0 Ω), open (0 S), and load (50 Ω)]. The analysis frequency range was 30 MHz to 1.5 GHz.

The static decay time was measured using an Electro-Tech Systems, 406D Static-Decay Meter that complies with the Federal Test Method 101D, Method 4046 and Military Standard Mil-B-81705C. The Static-Decay Meter was calibrated by the ESD Testing Laboratory of Electro-Tech Systems, (Glenside PA) prior to the measurements. The relative humidity of the measuring area was monitored at about 50% and temperature of 25°C.

An Electro-Metrics EM-2107A coaxial line was used to apply an electromagnetic plane-wave to the composite specimens (ASTM D4935). The EM-2107A test fixture was connected through coaxial cables to an Agilent Technologies N5230A PNA Series Network Analyzer. The EM SE, in decibels (dB), was determined as ten times the negative logarithmic ratio of the measured transmitted power with the material present (load specimen), $P_{T,W}$, to the transmitted power without the material present (reference specimen), $P_{T,WO}$.[26]

$$\text{EM SE (dB)} = -10 \log \frac{P_{T,W}}{P_{T,WO}} \quad (1)$$

Thus, each circular composite specimen was placed between the test fixtures and measured at frequencies from 30 MHz to 1.5 GHz. The sample diameter was 133 mm, whereas the thickness was about 2.5–3 mm ($n = 2$).

Tensile tests were carried out for the nanocomposites using the ASTM D638 Type V technique at room temperature, which requires dogbone-shaped specimens of 25 mm of gauge-length and 3 mm of width. The specimens were of 1 mm in thickness and were die-cut into the ASTM dogbone shape. An ATS Universal 900 tensile tester at across-head speed of 25 mm min^{-1} was used to test six replicates per nanocomposite type ($n = 6$).

RESULTS AND DISCUSSION

Nanomodifier Morphology and Properties

Figure 1 displays representative SEM micrographs of the different HT carbon modifiers used in this study. PR-19 HT and MWNT HT are fairly straight, as are P-55 CF, but these have a diameter about an order of magnitude greater than that of PR-19 HT, which in turn possess a diameter about one order of magnitude larger than that of MWNT HT. HCNT HTs have a similar diameter to that of PR-19 HT, but possess a predominantly helically coiled morphology. The as-received HCNT

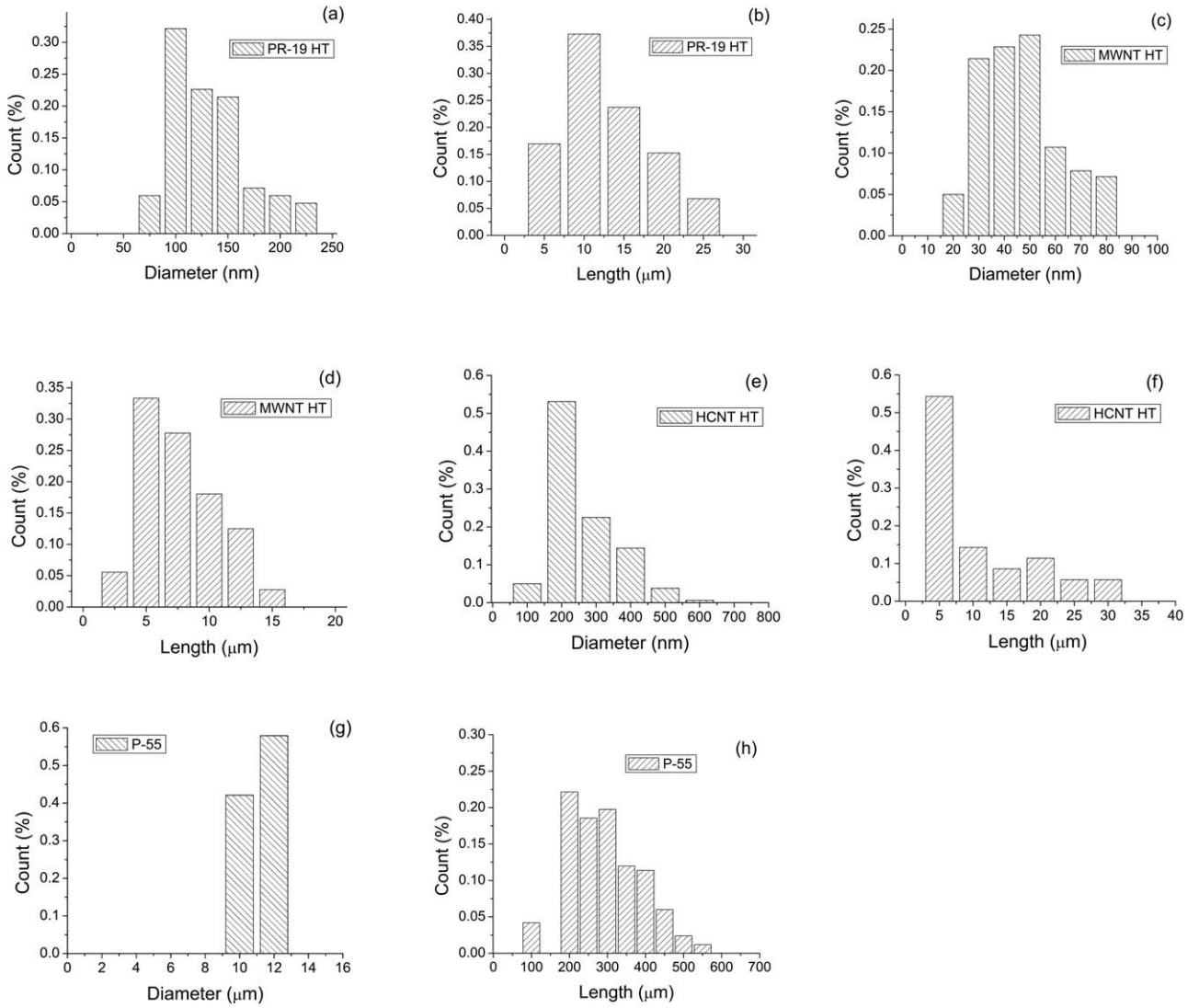

Figure 2. Results of the dimensional analysis of the carbon modifiers presented as histograms for the diameter and length distributions for (a, b) PR-19 HT, (c, d) MWNT HT, (e, f) HCNT HT, and (g, h) P-55 CF.

displayed a larger helical content, which was reduced by the heat treatment.

Figure 2 displays histograms of the diameter and length distributions of the modifiers obtained from image analysis of their SEM micrographs. PR-19 HT CNFs have a nominal diameter of 119 ± 8 nm and a length of 10 ± 2 μm, whereas MWNTs HT have a diameter of 42 ± 3 nm and length of 6 ± 1 μm (average ± 95% confidence intervals). HCNTs HT have a nominal diameter of 210 ± 15 nm and a length of 8.5 ± 2.5 μm. P-55 CFs have an average diameter of about 10 μm and lengths of about 100–500 μm. Thus, the average aspect ratios for the modifiers are about 86, 146, 41, and 30 for the PR-19 HT, MWNT HT, HCNT HT, and P-55 CF, respectively.

Figure 3 displays representative low-magnification SEM micrographs for the HT carbon nanomodifiers showing the original level of clustering of the modifiers before melt-mixing. Clusters as large as 300 μm were observed for PR-19 HT and MWNT HT, but their average cluster diameters were 29.6 ± 11.0 μm and 27.1 ± 13.9 μm, respectively. The HCNT HT, on the other hand, displayed a smaller average cluster size of 17.5 ± 6.4 μm and a considerable fraction of them appeared as exfoliated HCNT HT; however, a few clusters as large as 100 μm could still be found.

Raman spectroscopy is sensitive to graphitic structures.[31] In carbonaceous materials, the most important peaks occur at about 1300 and 1650 cm^{-1} and are known as the D (disordered) and G (graphitic) bands. The ratio of the integrated intensities of the D peak to the G peak (Raman I_D/I_G ratio) varies inversely with the crystal width, L_a, and is a measure of the level of graphitic crystallinity ($L_a = 44\ [I_D/I_G]^{-1}$).[32] Figure 4 exhibits the Raman spectra for the four types of carbon modifiers. The Raman I_D/I_G ratios obtained from the relative areas under the D and G bands for the PR-19 HT, MWNT HT, HCNT HT

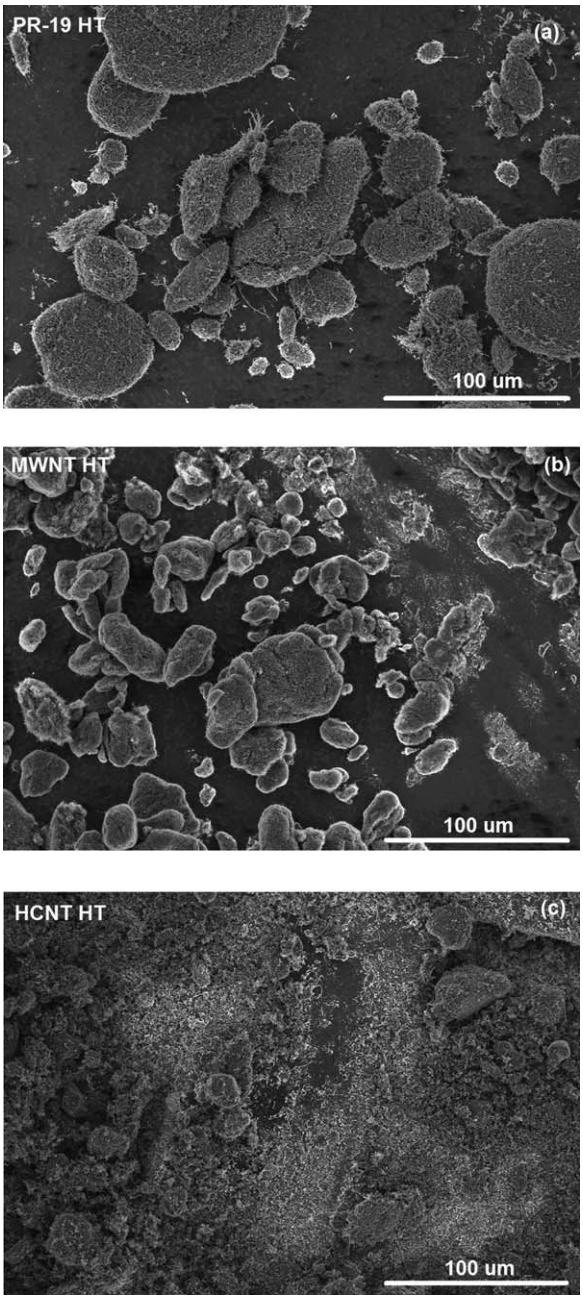

Figure 3. Representative low-magnification SEM of the HT carbon nanomodifiers forming initial clusters. (a) PR-19 HT, (b) MWNT HT, and (c) HCNT HT.

nanomodifiers, and P-55 CF were 0.96 ± 0.04 and 0.78 ± 0.11 and 1.68 ± 0.46, and 2.92 ± 0.08, respectively. P-55 CF showed the highest ratio, whereas HCNT HT displayed a slightly higher ratio than that of the other nanomodifiers. However, due to the large variability in I_D/I_G ratio of HCNT HT, these ratios were statistically not different ($I_D/I_G = 1$). These values should be contrasted to a significantly low value of 0.41 ± 0.02 for highly graphitic K1100 CF.

The assessment of graphitic crystallographic characteristics of carbonaceous materials can be primarily carried out by XRD.[27,33] For graphitic carbon, X-ray diffractograms display

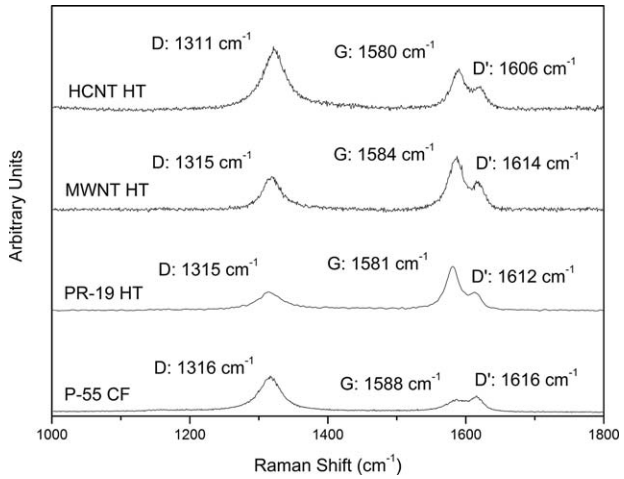

Figure 4. Raman spectra of the HT carbon modifiers. The spectra have been vertically shifted for clarity.

prominent peaks at about 26°, 42°, and 44° Bragg's angular positions (2θ) corresponding to reflections of the (002), (100), and (101) planes, respectively.[34] Of particular relevance is the angular position for the (002) peak, which determines the interlayer spacing between the graphene layers, d_{002}, and is a measure of the graphitic crystallinity. This is usually expressed in terms of level of graphitization, g_p, with reference to the interlayer spacing of 0.3354 nm for fully crystalline graphite and 0.344 nm for "turbostratic graphite"[34]:

$$g_p = \frac{0.3440 \text{ nm} - d_{002}}{0.3440 \text{ nm} - 0.3354 \text{ nm}} \times 100\% \quad (2)$$

From XRD, the Bragg's angles of the peaks corresponding with the (002), (100), and (101) planes of the graphitic structure of the modifiers are shown in Figure 5. The 2θ peaks for (002) planes were located in the range from 26.0° to 26.3°, whereas the 2θ peaks at 28.44°, 47.30°, and 56.12° were for the (111), (220), and (311) crystalline planes in the NIST-calibration grade

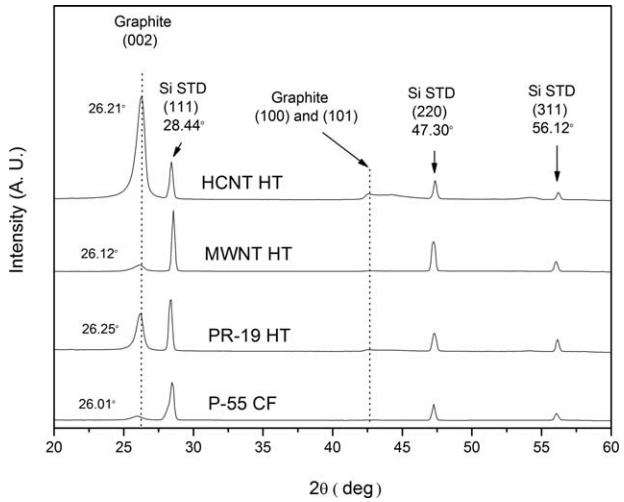

Figure 5. X-ray diffractograms of the HT carbon modifiers. A small quantity of NIST-calibration grade silicon was added to the samples for accurate determination of 2θ angles of various peaks.

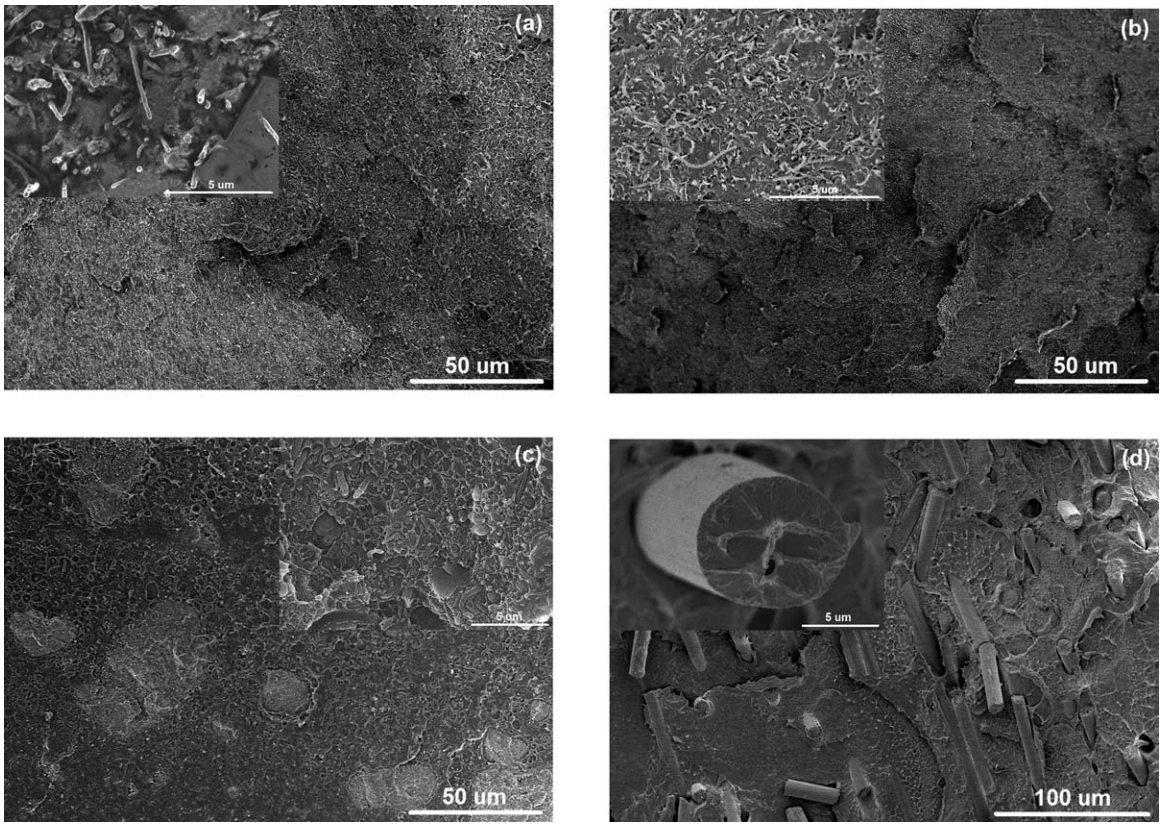

Figure 6. Representative SEM of the cross-section of the composites at 10 vol % (a) PR-19 HT, (b) MWNT HT, (c) HCNT HT, and (d) P-55 CF. Insets display the microstructure at higher magnification.

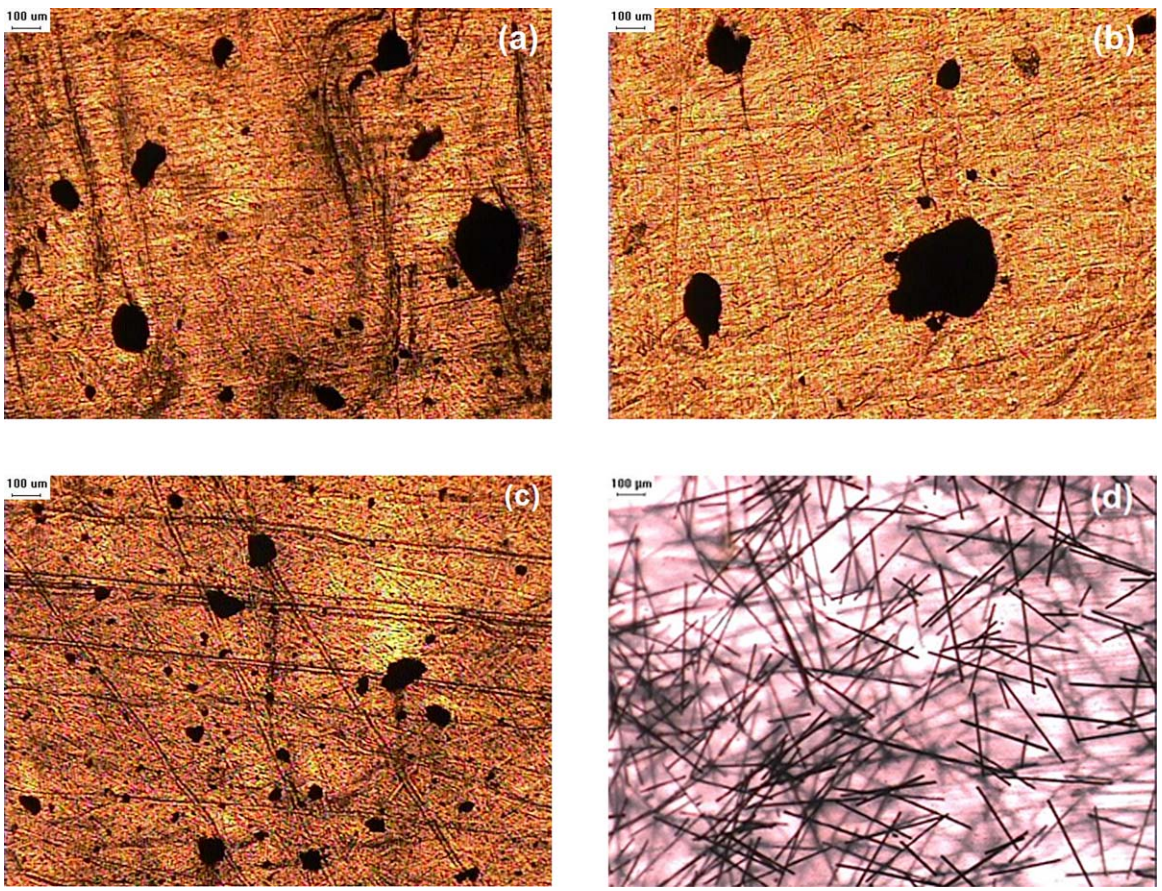

Figure 7. Representative light micrographs of the surface of the diluted composites at 1 vol %, (a) PR-19 HT, (b) MWNT HT, (c) HCNT HT, and (d) P-55 CF. [Color figure can be viewed in the online issue, which is available at wileyonlinelibrary.com.]

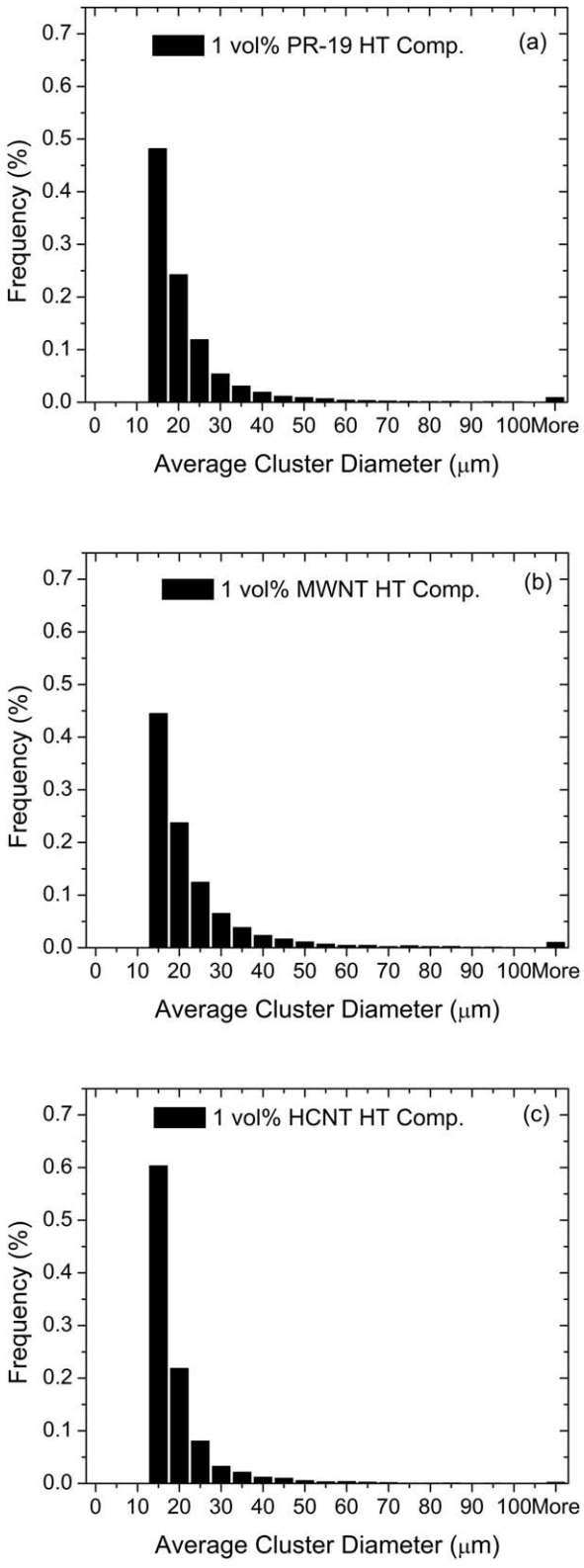

Figure 8. Cluster size distributions in 1 vol % diluted nanocomposites. (a) PR-19 HT comp., (b) MWNT HT comp., and (c) HCNT HT comp.

silicon added externally for confirming the accurate location of the graphitic peaks. The nanomodifiers all displayed a 2θ peak at around 26.20° for a graphitization level of about 40–60%. P-55 CF displayed a slightly lower 2θ position at 26.01° for the (002) graphitic peak, which corresponds to a lower graphitization level of about 20%. These results are consistent with the Raman results.

The BEC of the modifiers was measured at 3226 ± 787, 3571 ± 1246, and 1754 ± 346 Sm^{-1} for PR-19 HT, MWNT HT, and HCNT HT, respectively. Likewise, the bulk thermal conductivity of the nanomodifiers was 0.295 ± 0.010 Wm^{-1} K^{-1} for PR-19 HT, 0.473 ± 0.007 Wm^{-1} K^{-1} for MWNT HT, and 0.155 ± 0.018 Wm^{-1} K^{-1} for HCNT HT. These results indicate that differences in the crystallinity of the modifiers influence their transport properties. Nonetheless, all transport properties of these modifiers fall within the same order of magnitude (i.e., $5 \times 10^2 - 5 \times 10^3$ Sm^{-1}, 0.1–1.0 Wm^{-1} K^{-1}).

Composite Morphology

Figure 6 displays representative SEM micrographs for the composites at 10 vol % modifier content. The PR-19 HT-, MWNT HT-, and P-55-based composites appear uniformly mixed and no significant clusters can be observed. In contrast, HCNT HT-based composites retained several HCNT HT clusters as large as 100 μm. In fact, this cluster size observed in the composites is comparable to the size of the largest HCNT HT agglomerates before melt-mixing (~100 μm) as observed in Figure 3(c). This is likely a consequence of the helical morphology of the HCNT HT that resulted in significant entanglements, which hinder cluster breakage (rupture) and lead to similar cluster size prior to and after mixing.[21]

Figure 7 shows the light micrographs of the diluted composites at 1 vol %. In contrast to the SEM micrographs, light microscopy, that can capture a much larger observed area (although at a lower magnification), displayed clusters of nanomodifiers for all three types of nanocomposites. Only a few clusters were observed for the PR-19 HT- and MWNT HT-nanocomposites, although some were fairly large (~300 μm). In contrast, in the diluted HCNT HT nanocomposites, a larger number of relatively smaller clusters were observed. The diluted P-55 CF composites displayed a random in-plane distribution of the fibers, but there are still regions in which higher concentrations of CF were observed.

Figure 8 displays the average cluster size distribution of the nanomodifiers in the 1 vol % diluted composite films obtained by image analysis of their light micrographs. The clusters in the PR-19 HT diluted composites had a diameter of 20.7 ± 15.4 μm. For the MWNT HT diluted composite films, a diameter of 21.5 ± 12.9 μm was measured. The HCNT HT dilute nanocomposites displayed an average diameter of 16.9 ± 6.3 μm. These values are consistent with the visual assessment previously made. Although, the coiled morphology of the HCNT HT favors clustering, the relatively smaller average cluster size in HCNT HT composites may be a consequence of the lower aspect ratio of the HCNT HT.

A measure of the nondispersed phase can be obtained as the ratio of the total cluster area, A_C, to the total inspected area, A_T.[21] This ratio is proportional to the volume fraction of the clusters in the composite.[21] Thus, PR-19 HT, MWNT

Table I. Intrinsic Properties of Four Types of Modifiers as Compared with the Conductivity of Their Batch-Mixed Composites at 10 vol % Modifier Content

Modifier	Raman I_D/I_G ratio	Bragg's angle (°)	Level of graphitization (%)	Bulk electrical conductivity (Sm^{-1})	Bulk thermal conductivity ($Wm^{-1}\ K^{-1}$)	Aspect ratio (L/D)	In-plane electrical conductivity (Sm^{-1}) composites 10 vol %	Through-plane thermal conductivity ($Wm^{-1}\ K^{-1}$) composites 10 vol %
PR-19 HT	0.96 ± 0.04	26.25	55	3226 ± 787	0.295 ± 0.010	63–108	$20.4 \pm 3.3 \times 10^{0}$	0.855 ± 0.029
MWNT HT	0.78 ± 0.11	26.12	40	3571 ± 1246	0.473 ± 0.007	111–180	$33.5 \pm 5.6 \times 10^{0}$	1.022 ± 0.023
HCNT HT	1.68 ± 0.46	26.21	50	1754 ± 346	0.155 ± 0.018	26–56	$3.7 \pm 1.6 \times 10^{-3}$	0.555 ± 0.003
P-55	2.92 ± 0.08	26.01	20	862 ± 204	-	24–35	$5.0 \pm 1.8 \times 10^{0}$	0.562 ± 0.009

Ranges represent 95% confidence intervals.

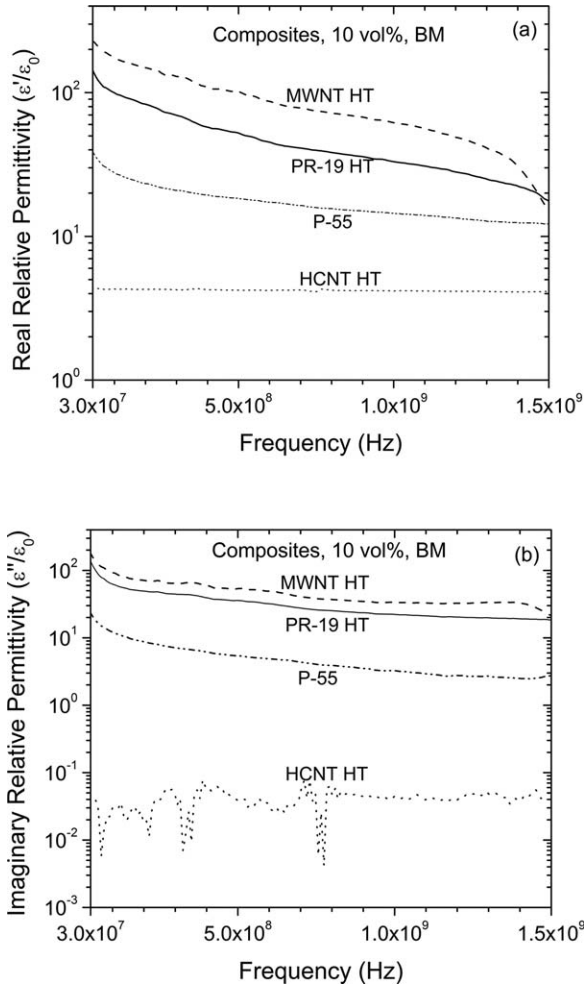

Figure 9. Relative (a) real and (b) imaginary electrical permittivity of representative composites.

HT, and HCNT HT diluted nanocomposites exhibited ratio values of $^{A_C}/_{A_T}$ of 0.379 ± 0.075, 0.378 ± 0.042, and 0.207 ± 0.064, respectively. Although the SEM micrographs for the HCNT HT nanocomposites at 10 vol % displayed clusters, their predominant cluster size and cluster area ratio were lower than those for the PR-19 HT and MWNT HT nanocomposites. These results quantitatively confirm that a larger number of relatively smaller isolated clusters are present in the HCNT HT nanocomposites.

Composite Transport Properties

For polyolefin matrix nanocomposites, electrical percolation thresholds ranging from 2.5 to 7.5 vol % have been reported for CNFs and CNTs in literature studies where the conductivity of the composite is several orders higher than that of the pure resin, for example, 10^{-5} versus 10^{-15} Sm^{-1}.[8,28,35] However, a conductivity of 10^{-5} Sm^{-1} is insufficient for shielding purposes.[4,6,18,26,27,29] Therefore, for obtaining significant shielding effectiveness, it is necessary to increase modifier levels well beyond the percolation threshold. Because of this, and based on the results of our prior studies, the batch-mixed formulation of 10 vol % was chosen for a systematic evaluation of the shielding properties.[26,27]

Table II. Static Decay-Times for ESD of the Composites, Measured at 1% Cut-off and 50% Relative Humidity

10 vol % Composites	Decay time[a] (s)
PR-19 HT	0.01
MWNT HT	0.01
HCNT HT	1.50
P-55	0.01

[a] 1% cut-off.

Table I is a summary of the transport properties of the modifiers and their composites. The DC in-plane electrical conductivity of the 10 vol % nanocomposites was measured at $20.4 \pm 3.3 \times 10^0$, $33.5 \pm 5.6 \times 10^0$, $3.7 \pm 1.6 \times 10^{-3}$, and $5.0 \pm 1.8 \times 10^0$ Sm^{-1} ($n = 4$ in all cases) for the PR-19 HT, MWNT HT, HCNT HT, and P-55 composites, respectively. The composites were electrically percolated when compared with pure LLDPE with a conductivity of $7.0 \pm 1.1 \times 10^{-15}$ Sm^{-1}, which is 15 orders of magnitude lower than that of the composites. Similarly, the through-plane thermal conductivity of the composites (also shown in Table I) was 0.855 ± 0.029, 1.022 ± 0.023, 0.555 ± 0.003, and 0.562 ± 0.009 Wm^{-1} K^{-1} for the PR-19 HT, MWNT HT, HCNT HT, and P-55 composites, respectively.

The MWNT HT with the highest aspect ratio (L/D) led to composites with large percolating network and the highest conductivities. In contrast, HCNT HT, with a low aspect ratio and helical morphology, developed segregated microstructure, which prevented an effective electrical network interconnection, and led the lowest conductivities. The PR-19 HT and P-55 CF conductivities fall in between these two extremes as do their aspect ratios. Given that all four types of modifiers have similar intrinsic transport properties (i.e., same order of magnitude), and the processing conditions and concentration have been kept equal for the same polymeric matrix, the composite properties are primarily dependent on the morphological features of the modifiers.

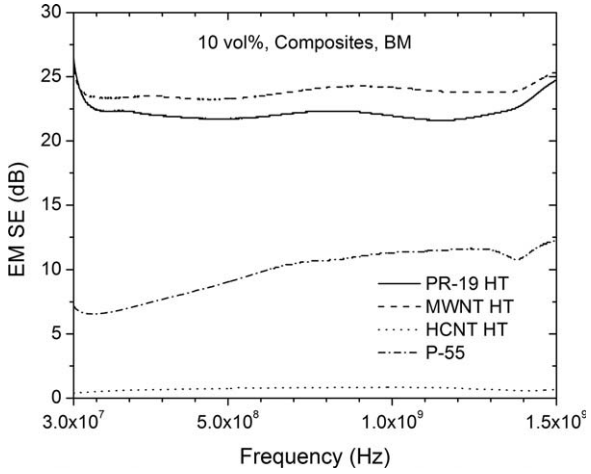

Figure 10. EM SE of representative 10 vol % composites over the frequency range of 30 MHz to 1.5 GHz.

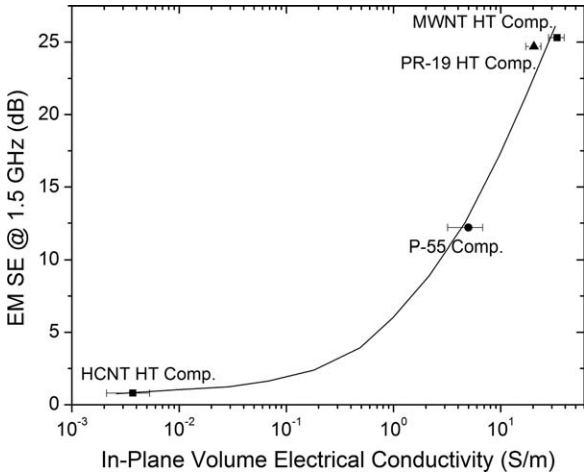

Figure 11. Plot showing a positive correlation between the EM SE @ 1.5 GHz and the corresponding in-plane electrical conductivity of the different composites. Solid line represents a typical trend.

The complex electrical permittivity of the nanocomposites ($\varepsilon = \varepsilon' - j\varepsilon'''$) is displayed in Figure 9, where $\varepsilon'/\varepsilon_0$ represents the relative real permittivity and $\varepsilon''/\varepsilon_0$ the relative imaginary permittivity. The real and imaginary permittivity of the nanocomposites displayed a generally decreasing behavior with respect to frequency. The MWNT HT nanocomposites exhibited an overall permittivity of 175-93 j at 100 MHz, decreasing to 15–21 j at 1.5 GHz. PR-19 HT nanocomposites permittivity decreased from 100-63 j at 100 MHz to 17–18 j at 1.5 GHz. In contrast, the permittivity of HCNT HT and P-55 composites was less frequency dependent at about 4-0.050 j and 12-3 j at 1.5 GHz, respectively (replication $n = 4$). Again, the composites containing modifiers with larger aspect ratios displayed higher permittivities. Particularly low was the permittivity of the HCNT HT nanocomposites, which was only slightly higher than that of the pure LLDPE ($\varepsilon/\varepsilon_0 \approx 2.3$). Such a low permittivity also reflects the poor electrical interconnectivity between the HCNT HT clusters.

ESD and Electromagnetic Shielding

The ESD characteristic of the nanocomposites in terms of the decay time for each nanocomposite type is displayed in Table II (1% of cut-off). The Military Standard requires that 99% of the initial induced charge be dissipated is <2 s for qualifying material per Mil-B-81705C. At 10 vol %, all types of composites were ESD dissipative and complied with the Mil-B-81705C requirements. This is not surprising since they all were in the percolated regime, and it is known that the electrostatic decay time increases as the conductivity of the material decreases.[36,37] Only, HCNT HT composites displayed, a slightly higher, but still dissipative, decay time of 1.5 s, which is consistent with its low electrical conductivity of only ~0.004 Sm^{-1}.

Figure 10 displays the EM SE of the composites. PR-19 HT nanocomposites possessed 24.7 dB of shielding, and MWNT HT nanocomposites a slightly larger value of 25.3 dB. P-55

Table III. Estimated EM SE for the Different Composites as Compared with the Measured EM SE Values

	PR-19 HT	MWNT HT	HCNT HT	P-55
Specimen thickness (mm)	3.0	2.6	2.5	2.4
In-plane electrical conductivity (Sm^{-1})	$20.4 \pm 3.3 \times 10^{0}$	$33.5 \pm 5.6 \times 10^{0}$	$3.7 \pm 1.6 \times 10^{-3}$	$5.0 \pm 1.8 \times 10^{0}$
Relative complex electrical permittivity @ 1.5 GHz	17.0−18.0j	15.0−21.0j	4.0−0.05j	12.0−3.0j
Relative magnetic permeability @ 1.5 GHz	1	1	1	1
Estimated EM SE (dB) @ 1.5 GHz	21.41 ± 1.45	24.47 ± 1.60	0.02 ± 0.01	8.56 ± 2.08
Measured EM SE (dB) @ 1.5 GHz	24.7	25.3	0.7	12.2

Ranges represent 95% confidence intervals.

composites exhibited 12.2 dB, whereas the lowest value of the set was of only 0.7 dB for the HCNT HT composites (all values at 1.5 GHz). Figure 11 displays the interrelationship between the EM SE and the in-plane conductivity of the composites. An increasing trend between the in-plane conductivity and the EM SE of the composites can be noted. These results are consistent with the electrical conductivity and permittivity measurements, that is, the larger the values of EM SE are consistent with the higher "lossy" properties of the composite (electrical conductivity and imaginary permittivity). In a recent study,[4] we have conducted an analysis of the shielding of plane-waves by the lossy properties of a quasi-homogeneous material. We have shown that the EM SE for a sample can be estimated from the in-plane electrical conductivity, σ, and the electrical permittivity, $\varepsilon = \varepsilon' - j\varepsilon''$, $(j = \sqrt{-1})$, of the material[4]:

$$\text{EM SE}_{\text{dB}} = -10\log\left|\left\{\frac{\frac{4\eta\eta_o}{(\eta_o+\eta)^2}\, e^{-\alpha t}}{1-\left(\frac{\eta-\eta_o}{\eta+\eta_o}\right)^2 e^{-2\alpha t}}\right\}^2\right| \quad (3)$$

where, t is the sample thickness, and η_o the intrinsic impedance of the vacuum with a value of $120\pi\ \Omega$. The intrinsic impedance, η, and attenuation constant, α, of the material respectively are:[4]

$$\eta = \sqrt{\frac{\mu}{\varepsilon' - \left(\varepsilon'' + \frac{\sigma}{\omega}\right)j}} \quad (4)$$

$$\alpha = \omega\sqrt{\frac{\mu\varepsilon'}{2}\left(\sqrt{1+\left[\frac{\left(\frac{\sigma}{\omega}+\varepsilon''\right)}{\varepsilon'}\right]^2}-1\right)} \quad (5)$$

where, μ, is the magnetic permeability of the material and, ω, the angular wave frequency.

Table III displays a summary of the estimated EM SE of the different composites at 1.5 GHz from the different material parameters. For the PR-19 HT and MWNT HT nanocomposites, the EM SE predictions are fairly consistent with the experimental values (within 10% error). For P-55 composites, their lower level of homogeneity led to a greater variation of about 30%. For the HCNT HT nanocomposites, due to their very low levels of conductivity and permittivity, the estimation was not accurate. Thus, for PR-19 HT and MWNT HT samples, the general trend of the EM SE dependency on the lossy properties is captured.

Mechanical Properties

Table IV displays the tensile properties of the different composites prepared in this study. At 10 vol %, PR-19 HT and MWNT HT nanocomposites displayed similar values for tensile modulus, strength, and ductility (measured as strain-to-failure). In contrast, HCNT HT composites were more flexible and more ductile than the other nanocomposites, whereas P-55 composites were much stiffer and significantly less ductile than others. The retention of ductility of the HCNT HT composites is likely due to the mechanical interlocking of the helical shape of the nanomodifier. This has also been reported by Lee et al.[25] when studying composites made of similar modifier morphologies to that of the HCNT HT. Although the nanocomposites were generally less flexible as compared to the pure LLDPE, consistent with other literature studies,[21,35–38] they still retained a fairly high strain-to-failure of about 165%, compared to about only 30% displayed by the P-55 composites.

CONCLUSIONS

The EM SE of the studied composites exhibited a direct dependence on the modifier morphology. As a result, MWHT HT,

Table IV. Tensile Properties for Composites at 10 vol % Modifier Content

	PR-19 HT	MWNT HT	HCNT HT	P-55
Apparent Modulus (MPa)	683 ± 105	696 ± 110	443 ± 58	1079 ± 88
Yield Stress (MPa)	16.5 ± 1.8	18.3 ± 1.8	13.3 ± 0.3	20.0 ± 1.5
Tensile Strength (MPa)	16.0 ± 2.5	17.7 ± 1.6	14.8 ± 1.7	8.0 ± 1.4
Elongation-at-break (%)	128 ± 49	114 ± 43	254 ± 62	32 ± 8

Ranges represent 95% confidence intervals.

whose aspect ratio was the largest of the studied set, displayed the largest conductivity, permittivity and shielding effectiveness (~24 dB) in its composite form. In contrast, the HCNT HT, due to their coiled shape and low aspect ratio, led to poorer network in the composites, which resulted in poor EM SE (<1 dB). Nevertheless, HCNT HT composites exhibited the highest ductility and flexibility of the studied set of composites, which is owed to the mechanical interlocking between the matrix and the helical coils. PR-19 HT and P-55 CF, both with intermediate aspect ratios and straight-shape morphology, led to composite properties that were intermediate between the two extremes. The microstructure of the composites was found to directly depend on the morphology of the carbon modifiers, which leads to the electrical network that the modifiers form within the matrix.

ACKNOWLEDGMENTS

This work made use of ERC Shared Facilities supported by the National Science Foundation under Award Number EEC-9731680.

REFERENCES

1. Tong, X. C. Advanced Materials and Design for Electromagnetic Interference Shielding; Taylor & Francis Group, LLC: United States of America, **2009**.
2. Paul, C. R. Introduction to Electromagnetic Compatibility; Wiley: United States of America, **1992**.
3. Ott, H. W. Electromagnetic Compatibility Engineering; Wiley: United States of America, **2009**.
4. Villacorta, B. S.; Hubing, T. H.; Ogale, A. A. *Compos. Sci. Technol.* **2013**, *89*, 158.
5. Kaiser, K. L. Electrostatic Discharge; Taylor & Francis Group LLC: United States of America, **2006**.
6. Villacorta, B. S.; McDowell, A.; Hubing, T. H.; Ogale, A. A. *Polym. Eng. Sci., to appear*, DOI 10.1002/pen.23901.
7. Al-Saleh, M. H.; Sundararaj, U. *Polym. Adv. Technol.* **2011**, *22*, 246.
8. Al-Saleh, M. H.; Sundararaj, U. *Carbon* **2009**, *47*, 1738.
9. Gelves, G.; Lin, B.; Sundararaj, U.; Haber, J. *Adv. Funct. Mater.* **2006**, *16*, 2423.
10. Al-Saleh, M. H.; Gelves, G. A.; Sundararaj, U. *Compos. A* **2011**, *42*, 92.
11. King, J. A.; Morrison, F. A.; Keith, J. M.; Miller, M. G.; Smith, R. C.; Cruz, M.; Neuhalfen, A. M.; Barton, R. L. *J. Appl. Polym. Sci.* **2006**, *101*, 2680.
12. Zhou, P.; Yu, W.; Zhou, C.; Liu, F.; Hou, L.; Wang, L. *J. Appl. Polym. Sci.* **2007**, *103*, 487.
13. Nanni, F.; Valentini, M. In Polymer-carbon nanotube composites, Preparation, properties and applications; McNally, T., Pötschke P., Eds.; Woodhead Publishing: Cambridge, UK, **2011**, Chapter *11*, pp 329–346.
14. Lozano, K.; Yang, S.; Zeng, Q. *J. Appl. Polym. Sci.* **2004**, *93*, 155.
15. Janda, N. B.; Keith, J. M.; King, J. A.; Perger, W. F.; Oxby, T. J. *J. Appl. Polym. Sci.* **2005**, *96*, 62.
16. Dani, A.; Ogale, A. A. *Compos. Sci. Technol.* **1996**, *56*, 911.
17. Dani, A.; Ogale, A. A. *Compos. Sci. Technol.* **1997**, *57*, 1355.
18. Villacorta, B. S.; Ogale, A. A. *Proc SPE ANTEC* **2011**, *11*, 0093.
19. Ling, Q.; Sun, J.; Zhao, Q.; Zhou, Q. *Mater. Sci. Eng. B* **2009**, *162*, 162.
20. Kaukonen, M.; Gulans, A.; Havu, P.; Kauppinen, E. *J. Comput. Chem.* **2012**, *33*, 652.
21. Kasaliwal, G. R.; Villmow, T.; Pegel, S.; Potschke, P. In Polymer-carbon nanotube composites, Preparation, properties and applications; McNally, T., Pötschke P., Eds.; Woodhead Publishing: Cambridge, UK, **2011**, Chapter *4*, pp 92.
22. Li, J.; Ma, P. C.; Chow, W. S.; To, C. K.; Tang, B. Z.; Kim, J.-K. *Adv. Funct. Mater.* **2007**, *17*, 3207.
23. Lee, S.; Kim, M.-S.; Ogale, A. A. *Polym. Eng. Sci.* **2010**, *50*, 93.
24. Lee, S.; Kim, T.; Ogale, A. A.; Kim, M. *Synth. Met.* **2007**, *157*, 644.
25. Lee, S.; Kim, M.; Ogale, A. A. *Polym. Eng. Sci.* **2010**, *50*, 93.
26. Villacorta Hernandez, B. Effect of Graphitic Carbon Nanomodifiers on the Electromagnetic Shielding Effectiveness of Linear Low Density Polyethylene Nanocomposites, PhD Thesis, Clemson University, Clemson, December **2013**, All Dissertations, Paper 1234.
27. Villacorta, B. S.; Ogale, A. A.; Hubing, T. H. *Polym. Eng. Sci.* **2013**, *53*, 417.
28. Lee, S.; Da , S.; Ogale, A. A.; Kim, M. *J. Phys. Chem. Solids* **2008**, *69*, 1407.
29. Villacorta, B. S.; Ogale, A. A. *Proc. SPE ANTEC* **2013**, *2013*, 1589729.
30. Singjai, P.; Changsarn, S.; Thongtem, S. *Mater. Sci. Eng. A* **2007**, *443*, 42.
31. Amer, M. S. Raman Spectroscopy for Soft Matter Applications; Wiley: United States of America, **2009**.
32. Lee S. Effect of Carbon Nanofibers on the Microstructure and Properties of Polymer Nanocomposites. PhD dissertation, Clemson University, **2007**.
33. He, B. B. Two-Dimensional X-Ray Diffraction; Wiley: United States of America, **2009**.
34. Burchell, T. D. Carbon Materials for Advanced Technologies; Elsevier Science: Netherlands, **1999**.
35. Morcon, M.; Simon, G. In Polymer-carbon nanotube composites, Preparation, properties and applications; McNally, T., Pötschke P., Eds.; Woodhead Publishing: Cambridge, UK, **2011**, Chapter *17*, pp 511–544.
36. Voldman, S. H. ESD: Physics and Devices; Wiley: Vermont, **2004**.
37. Pratt, T. H. Electrostatic Ignitions of Fires and Explosions; American Institute of Chemical Engineers: New York, **2000**.
38. Goh, S. H. In Polymer-carbon nanotube composites, Preparation, properties and applications; McNally, T., Pötschke P., Eds.; Woodhead Publishing: Cambridge, UK, **2011**, Chapter *12*, pp 347–375.